

An unidentified line in X-ray spectra of the Andromeda galaxy and Perseus galaxy cluster

A. Boyarsky¹, O. Ruchayskiy², D. Iakubovskiy^{3,4} and J. Franse^{1,5}

¹Instituut-Lorentz for Theoretical Physics, Universiteit Leiden, Niels Bohrweg 2, Leiden, The Netherlands

²Ecole Polytechnique Fédérale de Lausanne, FSB/ITP/LPPC, BSP, CH-1015, Lausanne, Switzerland

³Bogolyubov Institute of Theoretical Physics, Metrologichna Str. 14-b, 03680, Kyiv, Ukraine

⁴National University “Kyiv-Mohyla Academy”, Skovorody Str. 2, 04070, Kyiv, Ukraine

⁵Leiden Observatory, Leiden University, Niels Bohrweg 2, Leiden, The Netherlands

We identify a weak line at $E \sim 3.5$ keV in X-ray spectra of the Andromeda galaxy and the Perseus galaxy cluster – two dark matter-dominated objects, for which there exist deep exposures with the XMM-Newton X-ray observatory. Such a line was not previously known to be present in the spectra of galaxies or galaxy clusters. Although the line is weak, it has a clear tendency to become stronger towards the centers of the objects; it is stronger for the Perseus cluster than for the Andromeda galaxy and is absent in the spectrum of a very deep “blank sky” dataset. Although for individual objects it is hard to exclude the possibility that the feature is due to an instrumental effect or an atomic line of anomalous brightness, it is consistent with the behavior of a line originating from the decay of dark matter particles. Future detections or non-detections of this line in multiple astrophysical targets may help to reveal its nature.

The nature of dark matter (DM) is a question of crucial importance for both cosmology and for fundamental physics. As neutrinos – the only known particles that could be dark matter candidates – are known to be too light to be consistent with various observations (see e.g. [1] for a review), it is widely anticipated that a new particle should exist to extend the hot Big Bang cosmology paradigm to dark matter. Although many candidates have been put forward by particle physicists (see e.g. [2]), little is known experimentally about the properties of DM particles: their masses, lifetimes, and interaction types remain largely unconstrained. *A priori*, a given DM candidate can possess a decay channel if its lifetime exceeds the age of the Universe. Therefore, the search for a DM decay signal provides an important test to constrain the properties of DM in a model-independent way. For fermionic particles, one should search above the Tremaine-Gunn limit [3] ($\gtrsim 300$ eV). If the mass is below $2m_e c^2$, such a fermion can decay to neutrinos and photons, and we can expect two-body radiative decay with photon energy $E_\gamma = \frac{1}{2}m_{\text{DM}}$. Such particles can be searched for in X-rays (see [4] for review of previous searches). For each particular DM model, the particle’s mass, lifetime and other parameters are related by the requirement to provide the correct DM abundance. For example, for one very interesting DM candidate – the right-handed neutrino – this requirement restricts the mass range to 0.5 – 100 keV [4, 5]. A large part of the available parameter space for sterile neutrinos is fully consistent with all astrophysical and cosmological bounds [6], and it is important to probe it still further.

The DM decay line is much narrower than the spectral resolution of the present day X-ray telescopes and, as previous searches have shown, should be rather weak. The X-ray spectra of astrophysical objects are crowded with weak atomic and instrumental lines, not all of which may be known. Therefore, even if the exposure of available observations continues to increase, it is hard to exclude an astrophysical or instrumental origin of any weak line found in the spectrum of individual

object. However, if the same feature is present in the spectra of a number of different objects, and its surface brightness and relative normalization between objects is consistent with the expected behavior of the DM signal, this can provide much more convincing evidence about its nature.

The present paper takes a step in this direction. We present the results of the combined analysis of many XMM-Newton observations of two objects at different redshifts – the Perseus cluster and the Andromeda galaxy (M31) – together with a long exposure “blank sky” dataset. We study the 2.8–8 keV energy band and show that the only significant un-modeled excess that is present in the spectra of both M31 and Perseus is located at ~ 3.5 keV energy and the line in Perseus is correctly redshifted as compared to Andromeda (at 95% CL). The relative fluxes for the two objects are in agreement with what is known about their DM distributions. We also study surface brightness profiles of this line and find them consistent with expectations for a DM decay line. We do not detect such a line in the very deep “blank sky” dataset, which disfavors some of the scenarios for its instrumental origin (e.g. features in the effective area). The upper bound from this dataset is consistent with expectations for a DM signal that would come in this case primarily from the Milky Way halo. However, as the line is weak ($\sim 4\sigma$ in the combined dataset) and the uncertainties in DM distribution are significant, positive detections or strong constraints from more objects are clearly needed in order to determine the nature of this signal.¹

Below we summarize the details of our data analysis and then

¹ During our work we became aware that a similar analysis has been carried out by different group for a collection of galaxy clusters. When this paper was in preparation, the arXiv preprint [7] by this group appeared, claiming a detection of a spectral feature at the same energy from a number of clusters.

discuss the results.

Data analysis. We use the data obtained with the European Photon Imaging Camera (EPIC) of *XMM-Newton* (“XMM” in what follows), which consists of two MOS [8] and one PN [9] CCD camera. We start with the basic Observation Data Files and reduce them using the procedures `emproc` and `eproc` for the MOS and PN cameras (SAS v.13.0.0 [10]). Raw event lists exhibit significant time variability caused by the *soft solar protons* [11, 12]. To remove the time-variable component we use the 60 s histogram for the whole camera’s energy range and reject the intervals where count rates deviate by more than 1.5σ from the mean value (`espfilt` procedure from SAS). By this procedure we discard $\sim 40\%$ of total observation time. However, residual soft proton flares can produce weak line-like features in the spectra at positions where the effective area is non-monotonic (see e.g. [13]). To further filter the data, we apply the procedure described in [14], based on the comparison of high-energy count rates for “in-FoV” (10-15 arcmin off-center) and out-FoV CCD regions [15]. We selected only observations where the ratio of $F_{in} - F_{out} < 1.15$.²

Combined observation of M31 center. The Andromeda galaxy (M31) has been extensively observed with XMM. In this work we use ~ 2 Msec of raw exposure observations of M31 within the central 1.5° . For the list of individual observations see Table III.

The XMM archive contains 35 observations of the center of M31 (offset less than $1.5'$ from (RA,DEC) = (00h42m44.3s +41d16m09s)). Of these observations we have selected 29 where residual contamination of the background flares is low ($F_{in} - F_{out} < 1.15$). For the PN camera only 8 observations had passed this criterion. We have chosen to keep only the 26 MOS1 observations taken after the CCD6 was damaged [17, 18]. In what follows we work with 26 MOS1 + 29 MOS2 observations combined.

We co-add channel-by-channel all PHA files for all central observations of M31, using the `addspec` routine from `FTOOLS` [19]. It also produces ARF- and exposure-weighted response files `.rsp` – the product of `.rmf` and `.arf` files of each observation. Finally, we bin the resulting spectra by 60 eV (4 MOS PI channels). This bin size is a factor ~ 2 smaller than the spectral resolution of the XMM at these energies, which makes the bins roughly statistically independent.

Background modeling. We model the contribution of the instrumental (particle induced) background by a combination of an unfolded power law (described in `xspec11` by `powerlaw/b`) plus a number of narrow `gaussian` lines

at the positions of instrumental K- α lines (Cr, Mn, K, Fe, Ni, Ca, Cu) and Fe K β . The astrophysical component is modeled by a `powerlaw` and lines around 2.4 keV and 3.0 keV (Ar and S line complexes). We restrict our modeling to the energy interval 2–8 keV, see Fig. 1.

Result. The resulting spectrum shows a group of positive residuals around 3.5 keV (Fig. 1). Adding a thin Gaussian line at that energy reduces the total χ^2 by ~ 13 , see Table I (more than 3σ significance for extra 2 degrees of freedom). Examination of MOS1 and MOS2 observations individually shows that the line is present in both cameras with comparable flux.

M31 off-center observations. Next we select off-center observations of M31 that pass the criterion $F_{in} - F_{out} < 1.15$ and whose centers are located within $23.7' - 55.8'$ from the center of M31 (20 observations for both MOS1 and MOS2). The background was modeled as in the on-center case. None of the cameras have any detectable residual in the energy range 3.53 ± 0.03 keV. The 2σ upper bound on the flux is given in Table I.

Perseus cluster. If the candidate weak signal is of astrophysical (rather than instrumental) origin, we should be able to detect its redshift. To this end we have chosen the nearby Perseus cluster (Abell 426). At its redshift, $z = 0.0179$, the line’s centroid would be shifted by 63 eV. As the position of the line is determined with about 30 eV precision, one can expect to resolve the line’s shift with about 2σ significance.

We have taken 16 observations with the MOS1 and MOS2 cameras of the Perseus cluster (excluding two observations on-center; see Table II) and processed them in the same way as for M31. The flare removal procedure left 215 ksec of PN camera’s exposure, therefore we also used the PN observations for Perseus.

Background modeling. The resulting spectra were then added together and fitted to the combination of `vmekal` (with free abundances for Fe, Ni, Ar, Ca and S) plus (extragalactic) `powerlaw`. The unfolded background component `powerlaw/b` plus the several most prominent instrumental lines were added to the model (similar to the M31 case).

Results. The fit shows significant positive residuals at energies around 3.47 keV (in the detector frame). Adding a `zgauss` model with the redshift of the cluster improves the fit by $\Delta\chi^2 = 9.1$ (for 2 degrees of freedom: position and normalization). The line’s position is fully consistent with that of M31 (Table I). If we fix the position of the line to that of M31 and allow the redshift to vary, $z = 0$ provides a worse fit by $\Delta\chi^2 = 3.6$ and its best-fit value is close to $z = 0.0179$.

Blank-sky dataset. To further study the origin of the new line we combine *XMM-Newton* blank-sky observations from [20, 21] with observations of the Lockman Hole. The data were reduced similarly to the other datasets. After filtering of soft proton flares we obtained 382 MOS observations. A dataset

² Ref. [14] argued that $F_{in} - F_{out} < 1.3$ is a sufficient criterion for flare removal. We find that a stricter criterion is needed to reduce artificial line-like residuals due to small wiggles in the effective area [13, 16].

Dataset	Exposure [ksec]	$\chi^2/\text{d.o.f.}$	Line position [keV]	Flux 10^{-6} cts/sec/cm ²	$\Delta\chi^2$
M31 ON-CENTER	978.9	97.8/74	3.53 ± 0.025	$4.9_{-1.3}^{+1.6}$	13.0
M31 OFF-CENTER	1472.8	107.8/75	3.53 ± 0.03	$< 1.8 (2\sigma)$...
PERSEUS CLUSTER (MOS)	528.5	72.7/68	$3.50_{-0.036}^{+0.044}$	$7.0_{-2.6}^{+2.6}$	9.1
PERSEUS CLUSTER (PN)	215.5	62.6/62	3.46 ± 0.04	$9.2_{-3.1}^{+3.1}$	8.0
PERSEUS (MOS) + M31 ON-CENTER	1507.4	191.5/142	$3.518_{-0.022}^{+0.019}$	$8.6_{-2.3}^{+2.2}$ (Perseus) $4.6_{-1.4}^{+1.4}$ (M31)	25.9 (3 dof)
BLANK-SKY	15700.2	33.1/33	3.53 ± 0.03	$< 0.7 (2\sigma)$...

TABLE I: Basic properties of combined observations used in this paper. Second column denotes the sum of exposures of individual observations. The last column shows change in $\Delta\chi^2$ when 2 extra d.o.f. (position and flux of the line) are added. The energies for Perseus are quoted in the rest frame of the object.

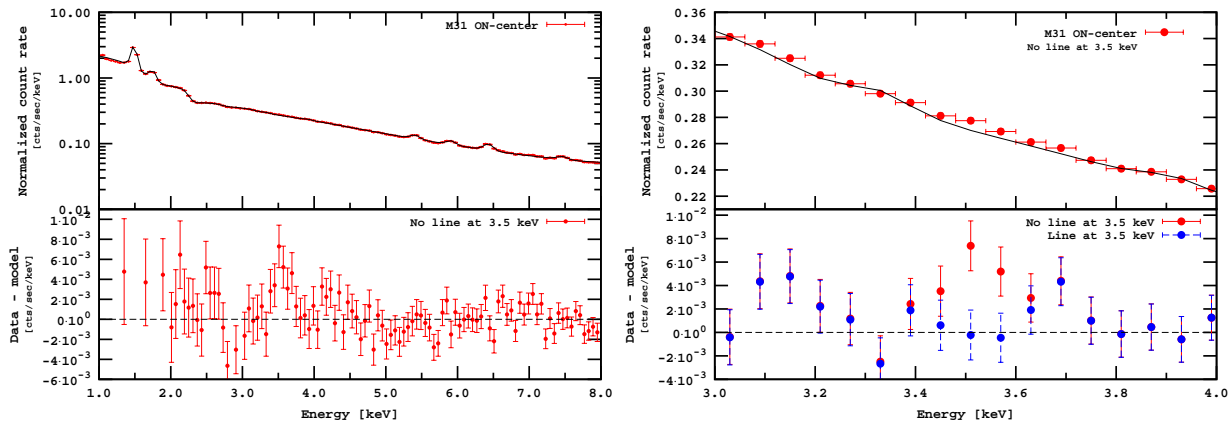


FIG. 1: *Left*: Folded count rate (top) and residuals (bottom) for the MOS spectrum of the central region of M31. Statistical Y-errorbars on the top plot are smaller than the point size. The line around 3.5 keV is *not added*, hence the group of positive residuals. *Right*: zoom onto the line region.

with such a large exposure requires special analysis (as described in [16]). This analysis did not reveal any line-like residuals in the range 3.45–3.58 keV with the 2σ upper bound on the flux being 7×10^{-7} cts/cm²/sec. The closest detected line-like feature ($\Delta\chi^2 = 4.5$) is at $3.67_{-0.05}^{+0.10}$ keV, consistent with the instrumental Ca $K\alpha$ line.³

Combined fit of M31 + Perseus. Finally, we have performed a simultaneous fit of the on-center M31 and Perseus datasets (MOS), keeping common position of the line (in the rest-frame) and allowing the line normalizations to be different. The line improves the fit by $\Delta\chi^2 = 25.9$ (Table I), which constitutes a 4.4σ significant detection for 3 d.o.f.

Results and discussion. We identified a spectral feature at $E = 3.518_{-0.022}^{+0.019}$ keV in the combined dataset of M31 and Perseus that has a statistical significance 4.4σ and does not coincide with any known line. Next we compare its properties with the expected behavior of a DM decay line.

The observed brightness of a decaying DM line should be proportional to the dark matter column density $\mathcal{S}_{\text{DM}} = \int \rho_{\text{DM}} dl$ – integral along the line of sight of the DM density distribution:

$$F_{\text{DM}} \approx 2.0 \times 10^{-6} \frac{\text{cts}}{\text{cm}^2 \cdot \text{sec}} \left(\frac{\Omega_{\text{fov}}}{500 \text{ arcmin}^2} \right) \times \left(\frac{\mathcal{S}_{\text{DM}}}{500 M_{\odot}/\text{pc}^2} \right) \frac{10^{29} \text{ s}}{\tau_{\text{DM}}} \left(\frac{\text{keV}}{m_{\text{DM}}} \right). \quad (1)$$

M31 and Perseus brightness profiles. Using the line flux of the center of M31 and the upper limit from the off-center observations we constrain the spatial profile of the line. The DM distribution in M31 has been extensively studied (see an overview in [13]). We take NFW profiles for M31 with concentrations $c = 11.7$ (solid line, [22]) and $c = 19$ (dash-dotted line). For each concentration we adjust the normalization so that it passes through first data point (Fig. 2). The $c = 19$ profile was chosen to intersect the upper limit, illustrating that the obtained line fluxes of M31 are fully consistent with the density profile of M31 (see e.g. [22, 24, 25] for a $c = 19 - 22$ model of M31).

³ Previously this line has only been observed in the PN camera [9].

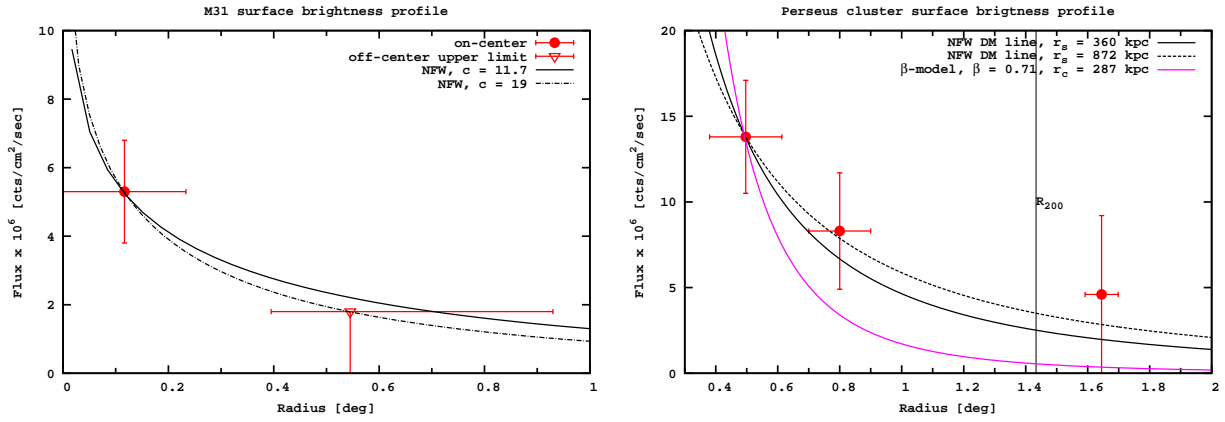


FIG. 2: The line’s brightness profile in M31 (left) and the Perseus cluster (right). An NFW DM distribution is assumed, the scale r_s is fixed to its best-fit values from [22] (M31) or [23] (Perseus) and the overall normalization is adjusted to pass through the left-most point.

For the Perseus cluster the observations can be grouped in 3 radial bins by their off-center angle. For each bin we fix the line position to its average value across Perseus (3.47 ± 0.07 keV). The obtained line fluxes together with 1σ errors are shown in Fig. 2. For comparison, we draw the expected line distribution from dark matter decay using the NFW profile of [23] (best fit value $r_s = 360$ kpc, black solid line; 1σ upper bound $r_s = 872$ kpc, black dashed line). The isothermal β -profile from [26] is shown in magenta. The surface brightness profile follows the expected DM decay line’s distribution in Perseus.

Finally, we compare the predictions for the DM lifetime from the two objects. The estimates of the average column density within the central part of M31 give $\mathcal{S}(r_s) \sim 200 - 600 M_\odot/\text{pc}^2$ [13]. The column density of clusters follows from the $c - M$ relation [27–29]. Considering the uncertainty on the profile and that our observations of Perseus go beyond r_s , the average column density in the region of interest is within $\bar{\mathcal{S}} \sim 100 - 600 M_\odot/\text{pc}^2$. Therefore the signal from Perseus can be both stronger and weaker than that of M31, by 0.2 – 3.0. This is consistent with the ratio of measured flux from Perseus to M31 0.7 – 2.7.

If DM is made of right-handed (sterile) neutrinos [30], the lifetime is related to its interaction strength (*mixing angle*):

$$\tau_{\text{DM}} = \frac{1024\pi^4}{9\alpha G_F^2 \sin^2(2\theta) m_{\text{DM}}^5} 7.2 \times 10^{29} \text{ sec} \left[\frac{10^{-8}}{\sin^2(2\theta)} \right] \left[\frac{1 \text{ keV}}{m_{\text{DM}}} \right]^5.$$

Using the data from M31 we obtain the mass $m_{\text{DM}} = 7.06 \pm 0.05$ keV and the mixing angle in the range $\sin^2(2\theta) = (2.2 - 20) \times 10^{-11}$. This value is consistent with previous bounds, Fig. 4. This means that sterile neutrinos should be produced resonantly [31–33], which requires the presence of significant lepton asymmetry in primordial plasma at temperatures few hundreds MeV. This produces restrictions on parameters of

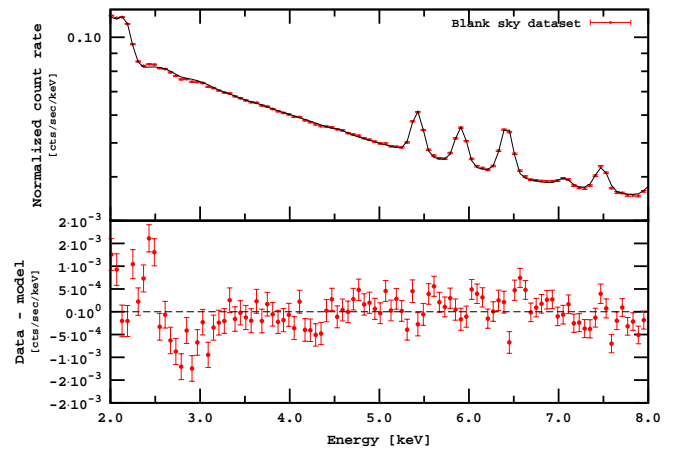


FIG. 3: Blank sky spectrum and residuals.

the ν MSM.

The position and flux of the discussed weak line are inevitably subject to systematical uncertainties. There are two weak instrumental lines (K $K\alpha$ at 3.31 keV and Ca $K\alpha$ at 3.69 keV), although formally their centroids are separated by more than 4σ . Additionally, the region below 3 keV is difficult to model precisely, especially at large exposures, due to the presence of the absorption edge and galactic emission. However, although the residuals below 3 keV are similar between the M31 dataset (Fig. 1) and the blank sky dataset (Fig. 3), the line is *not detected* in the latter. Although the count rate at these energies is 4 times larger for M31, the exposure for the blank sky is 16 times larger. This disfavors the interpretation of the line as due to a wiggle in the effective area. The properties of this line are consistent (within uncertainties) with the DM interpretation. To reach a conclusion about its nature, one will need to find more objects that give a detection or where non-observation of the line will put tight constraints on its properties. The forthcoming *Astro-H* mission [34] has sufficient spectral resolution to spectrally resolve the line against other nearby features and

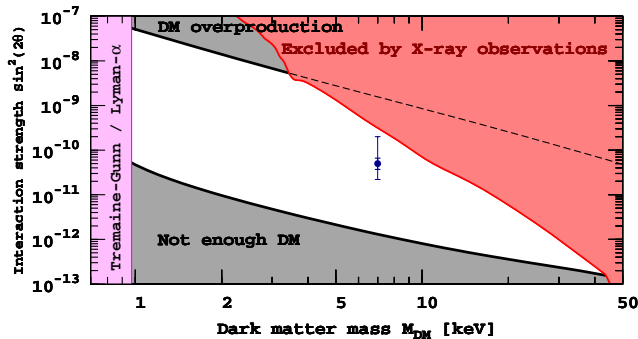


FIG. 4: Constraints on sterile neutrino DM within ν MSM [4]. The blue point would correspond to the best-fit value from M31 if the line comes from DM decay. Thick errorbars are $\pm 1\sigma$ limits on the flux. Thin errorbars correspond to the uncertainty in the DM distribution in the center of M31.

to detect the candidate line in the “strong line” regime [35]. In particular, *Astro-H* should be able to resolve the Milky Way halo’s DM decay signal and therefore all its observations can be used. Failure to detect such a line will rule out the DM origin of the Andromeda/Perseus signal presented here.

Acknowledgments. We thank D. Malyshev for collaboration; A. Neronov for useful critical comments; M. Shaposhnikov and M. Lovell for reading the manuscript and providing comment. The work of D. I. was supported by part by the the Program of Cosmic Research of the National Academy of Sciences of Ukraine and the State Programme of Implementation of Grid Technology in Ukraine.

-
- [1] A. Boyarsky, O. Ruchayskiy, and D. Iakubovskyi, *JCAP* **0903**, 005 (2009).
- [2] J. L. Feng, *ARA&A* **48**, 495 (2010).
- [3] S. Tremaine and J. E. Gunn, *Phys. Rev. Lett.* **42**, 407 (1979).
- [4] A. Boyarsky, D. Iakubovskyi, and O. Ruchayskiy, *Phys. Dark Univ.* **1**, 136 (2012).
- [5] A. Boyarsky, O. Ruchayskiy, and M. Shaposhnikov, *Ann. Rev. Nucl. Part. Sci.* **59**, 191 (2009).
- [6] A. Boyarsky, J. Lesgourgues, O. Ruchayskiy, and M. Viel, *Phys. Rev. Lett.* **102**, 201304 (2009).
- [7] E. Bulbul, M. Markevitch, A. Foster, R. K. Smith, M. Loewenstein, et al., 1402.2301 (2014).
- [8] M. J. L. Turner, A. Abbey, M. Arnaud, M. Balasini, M. Barbera, E. Belsole, P. J. Bennie, J. P. Bernard, G. F. Bignami, M. Boer, et al., *A&A* **365**, L27 (2001).
- [9] L. Strüder, U. Briel, K. Dennerl, R. Hartmann, E. Kendziorra, N. Meidinger, E. Pfeffermann, C. Reppin, B. Aschenbach, W. Bornemann, et al., *A&A* **365**, L18 (2001).
- [10] *Xmm-newton science analysis system*, <http://xmm.esa.int/sas/>.
- [11] A. M. Read and T. J. Ponman, *A&A* **409**, 395 (2003).
- [12] K. D. Kuntz and S. L. Snowden, *A&A* **478**, 575 (2008).
- [13] A. Boyarsky, O. Ruchayskiy, D. Iakubovskyi, M. G. Walker, S. Riemer-Sørensen, and S. H. Hansen, *MNRAS* **407**, 1188 (2010).
- [14] A. De Luca and S. Molendi, *Astron. Astrophys.* **419**, 837 (2004).
- [15] *Fin_over_fout public script, v. 1.1*, http://xmm.vilspa.esa.es/external/xmm_sw_cal/background/Fin_over_Fout.
- [16] D. Iakubovskyi, Ph.D. thesis, Leiden University (2013).
- [17] T. Abbey, J. Carpenter, A. Read, A. Wells, Xmm Science Centre, and Swift Mission Operations Center, in *The X-ray Universe 2005*, edited by A. Wilson (2006), vol. 604 of *ESA Special Publication*, p. 943.
- [18] *Xmm-newton epic mos1 ccd6 update*, http://xmm.esac.esa.int/external/xmm_news/items/MOS1-CCD6/.
- [19] Irby, B., The ftools webpage, *HeaSoft*, <http://heasarc.gsfc.nasa.gov/docs/software/ftools/ftools.menu.html> (2008).
- [20] J. A. Carter and A. M. Read, *A&A* **464**, 1155 (2007).
- [21] D. B. Henley and R. L. Shelton, *Astrophys.J.Suppl.* **202**, 14 (2012).
- [22] E. Corbelli, S. Lorenzoni, R. A. M. Walterbos, R. Braun, and D. A. Thilker, *A&A* **511**, A89 (2010).
- [23] A. Simionescu, S. W. Allen, A. Mantz, N. Werner, Y. Takei, R. G. Morris, A. C. Fabian, J. S. Sanders, P. E. J. Nulsen, M. R. George, et al., *Science* **331**, 1576 (2011).
- [24] L. Chemin, C. Carignan, and T. Foster, *Astrophys. J.* **705**, 1395 (2009).
- [25] M. A. Sanchez-Conde, M. Cannoni, F. Zandanel, M. E. Gomez, and F. Prada, *JCAP* **1112**, 011 (2011).
- [26] O. Urban, A. Simionescu, N. Werner, S. Allen, S. Ehlert, et al., *MNRAS* **437**, 3939 (2014).
- [27] A. Boyarsky, A. Neronov, O. Ruchayskiy, and I. Tkachev, *Phys. Rev. Lett.* **104**, 191301 (2010).
- [28] L. J. King and J. M. G. Mead, *MNRAS* **416**, 2539 (2011).
- [29] R. Mandelbaum, U. Seljak, and C. M. Hirata, *JCAP* **0808**, 006 (2008).
- [30] S. Dodelson and L. M. Widrow, *Phys. Rev. Lett.* **72**, 17 (1994).
- [31] X.-d. Shi and G. M. Fuller, *Phys. Rev. Lett.* **82**, 2832 (1999).
- [32] M. Shaposhnikov, *JHEP* **08**, 008 (2008).
- [33] M. Laine and M. Shaposhnikov, *JCAP* **6**, 31 (2008).
- [34] T. Takahashi, K. Mitsuda, R. Kelley, H. Aharonian, F. Aarts, et al., 1210.4378 (2012).
- [35] A. Boyarsky, J. W. den Herder, A. Neronov, and O. Ruchayskiy, *Astropart. Phys.* **28**, 303 (2007).

Appendix A: Supplementary material

	ObsID	Off-axis angle arcmin	Cleaned exposure MOS1/MOS2 [ksec]	FoV [arcmin ²] MOS1/MOS2	$F_{in}-F_{out}$
1	0305690301	22.80	18.6 / 18.6	473.6 / 574.3	1.266 / 1.340
2	0085590201	25.01	40.1 / 40.5	564.6 / 572.1	1.290 / 1.336
3	0204720101	27.87	14.1 / 14.5	567.7 / 574.5	2.373 / 2.219
4	0673020401	29.48	15.6 / 17.6	479.6 / 574.0	1.318 / 1.331
5	0405410201	29.52	16.1 / 16.6	480.8 / 573.9	1.354 / 1.366
6	0305690101	29.54	25.1 / 25.4	476.0 / 573.5	1.231 / 1.247
7	0405410101	31.17	15.8 / 16.8	481.8 / 572.9	1.235 / 1.195
8	0305720101	31.23	11.5 / 11.8	476.8 / 573.9	1.288 / 1.296
9	0673020301	36.54	13.9 / 15.4	485.4 / 573.8	1.211 / 1.304
10	0305690401	36.75	25.9 / 26.0	479.1 / 573.8	1.158 / 1.156
11	0305720301	41.92	16.7 / 17.5	464.7 / 573.6	1.433 / 1.447
12	0151560101	47.42	23.7 / 23.6	572.1 / 573.6	1.294 / 1.206
13	0673020201	53.31	22.8 / 23.4	479.5 / 573.9	1.262 / 1.228
14	0204720201	54.11	22.4 / 22.9	564.0 / 573.2	1.153 / 1.195
15	0554500801	95.45	15.0 / 15.3	480.8 / 572.7	1.098 / 1.113
16	0306680301	101.88	12.3 / 13.0	468.1 / 574.0	1.177 / 1.089

TABLE II: Parameters of the *XMM-Newton* spectra of Perseus cluster used in our analysis. The observations are sorted by off-axis angle from the center of the Perseus cluster. Two observations on-center (ObsIDs 0305780101 and 0085110101) are not included in the analysis. The difference in FoVs between MOS1 and MOS2 cameras is due to the loss CCD6 in MOS1 camera. The parameter $F_{in}-F_{out}$ (last column) estimates the presence of residual soft protons according to the procedure of [14] is also shown. Note, however, that for the bright extended sources, such an estimate is not appropriate, see http://xmm2.esac.esa.int/external/xmm_sw_cal/background/epic_scripts.shtml for details).

	ObsID	Off-axis angle	Cleaned exposure		FoV [arcmin ²]	F_{in} - F_{out}
		arcmin	MOS1/MOS2 [ksec]	MOS1/MOS2		
1	0405320501	0.02	12.3/13.6	480.6/573.2	1.132/1.039	
2	0405320701	0.02	14.8/14.9	480.7/572.8	1.046/1.057	
3	0405320801	0.02	13.1/13.1	488.2/573.0	1.160/1.117	
4	0405320901	0.02	15.5/15.6	488.0/574.3	1.099/1.065	
5	0505720201	0.02	25.2/26.2	485.6/572.1	1.079/1.057	
6	0505720301	0.02	25.4/24.3	486.0/573.9	1.129/1.105	
7	0505720401	0.02	19.9/20.2	488.6/573.1	1.113/1.108	
8	0505720501	0.02	12.9/13.9	480.3/574.1	1.151/1.064	
9	0505720601	0.02	20.2/20.4	488.3/571.4	1.085/1.108	
10	0551690201	0.02	20.5/20.3	486.5/574.2	1.099/1.072	
11	0551690301	0.02	19.7/19.4	479.3/573.0	1.109/1.117	
12	0551690501	0.02	16.9/18.4	486.3/573.2	1.095/1.109	
13	0600660201	0.02	17.4/17.5	487.0/572.9	1.080/1.041	
14	0600660301	0.02	16.1/16.1	488.6/572.0	1.054/1.041	
15	0600660401	0.02	15.0/15.5	479.9/573.1	1.078/1.072	
16	0600660501	0.02	13.5/14.3	488.2/573.4	1.079/1.083	
17	0600660601	0.02	15.2/15.1	481.8/573.6	1.073/1.041	
18	0650560201	0.02	21.0/21.3	488.1/573.3	1.198/1.140	
19	0650560301	0.02	26.9/29.0	487.9/572.6	1.082/1.095	
20	0650560401	0.02	12.4/13.5	488.0/573.1	1.157/1.069	
21	0650560501	0.02	15.8/21.6	487.8/573.4	1.162/1.114	
22	0650560601	0.02	20.8/21.5	487.5/572.2	1.085/1.068	
23	0674210201	0.02	19.6/19.6	478.6/573.3	1.094/1.083	
24	0674210301	0.02	14.9/15.0	488.1/573.6	1.052/1.043	
25	0674210401	0.02	17.9/18.1	485.7/572.7	1.071/1.081	
26	0674210501	0.02	16.2/16.3	488.8/573.5	1.192/1.139	
27	0202230201	1.44	18.3/18.4	567.1/572.8	1.089/1.108	
28	0202230401	1.44	17.0/17.1	566.5/573.6	1.118/1.109	
29	0202230501	1.44	9.2/9.4	568.1/574.1	1.048/1.129	
30	0402560201	23.71	16.0/16.6	478.7/574.0	1.096/1.095	
31	0505760201	23.71	35.2/38.6	476.6/571.6	1.065/1.058	
32	0511380201	23.71	15.3/15.4	485.0/572.7	1.126/1.047	
33	0511380601	23.71	14.8/17.2	485.4/573.1	1.041/1.074	
34	0402560901	24.18	42.4/42.9	475.0/572.8	1.118/1.071	
35	0672130101	24.24	73.0/78.6	473.1/572.8	1.088/1.064	
36	0672130501	24.24	22.7/25.4	477.0/574.8	1.097/1.110	
37	0672130601	24.24	67.8/67.3	471.8/571.4	1.115/1.101	
38	0672130701	24.24	70.7/74.3	484.8/573.5	1.076/1.052	
39	0410582001	26.29	13.2/13.9	485.4/575.0	1.073/1.030	
40	0402561001	28.81	48.0/49.4	478.4/572.5	1.084/1.042	
41	0402560301	30.34	43.9/45.7	474.6/573.1	1.037/1.027	
42	0505760301	39.55	41.0/41.3	485.0/570.8	1.022/1.022	
43	0402561101	39.56	44.8/44.8	478.7/571.4	1.121/1.067	
44	0404060201	42.94	19.1/19.1	480.7/573.7	0.993/1.045	
45	0402561201	47.37	38.1/39.2	478.5/573.3	1.077/1.034	
46	0402560501	49.06	48.8/50.6	487.2/572.9	1.102/1.079	
47	0511380301	49.06	31.5/31.0	482.0/572.3	1.105/1.082	
48	0151580401	50.89	12.3/12.3	567.2/574.1	1.131/1.020	
49	0109270301	55.81	25.5/25.0	562.6/571.6	1.110/1.106	

TABLE III: Parameters of the *XMM-Newton* spectra of M31 used in our analysis. The significant difference in FoVs between MOS1 and MOS2 cameras is due to the loss CCD6 in MOS1 camera. F_{in} - F_{out} parameter estimating the presence of residual soft protons according to procedure of [14] is also shown. First 29 observations are the dataset M31 ON, the remaining 20 – the dataset M31 OFF.